Coherent phonons in a Bi_2Se_3 film generated by an intense single-cycle THz pulse

A. A. Melnikov,[1,*] K. N. Boldyrev,[1] Yu. G. Selivanov,[2] V. P. Martovitskii,[2] S. V. Chekalin,[1] and E. A. Ryabov[1]
[1]*Institute for Spectroscopy RAS, Fizicheskaya 5, Troitsk, Moscow, 108840 Russia*
[2]*P. N. Lebedev Physics Institute RAS, Moscow, 119991 Russia*

(Received 25 September 2017; revised manuscript received 20 May 2018; published 14 June 2018)

We report an observation of coherent phonons of E_g^1, E_u^1, A_{1g}^1, and E_g^2 symmetry generated in a single-crystal film of Bi_2Se_3 by an intense single-cycle THz pulse. The atomic vibrations reveal themselves through periodic modulation of the refractive index of the film. The largest signal is detected at the frequency of 4.05 THz that corresponds to the E_g^2 mode. The generation of E_g^2 phonons is interpreted as resonant excitation of the Raman mode by the second harmonic of THz-driven nonlinear E_u^1 oscillator, the fundamental frequency of which (2.05 THz) is approximately half that of E_g^2. The origin of nonlinearity in this case is cubic lattice anharmonicity, while generation of E_g^1 (1.1 THz) and A_{1g}^1 (2.25 THz) phonons is a manifestation of quartic anharmonicity enhanced by the occasional combination relations between phonon frequencies in Bi_2Se_3.

DOI: 10.1103/PhysRevB.97.214304

I. INTRODUCTION

The development of laser sources of ultrashort pulses in midinfrared and terahertz domains has made it possible to study highly nonequilibrium states of matter previously inaccessible in experiments with pulses at visible wavelengths. Mid-IR and THz pulses can selectively excite low-energy degrees of freedom reducing concomitant population of higher-lying electronic states and avoiding generation of a hot thermalized electronic distribution. The exposure of a sample to intense low-frequency pulses tuned into resonance with a specific mode results in generation of a high-amplitude coherent wave packet on the timescales shorter than characteristic inverse rates of most relaxation processes. Such excited states are therefore convenient to use as models for studies of nonlinear effects, phase transitions, and interactions between rotational, vibrational, spin, and electronic degrees of freedom in their "pure" form. The number of applications of such an approach is growing fast [1,2]. Among them are the control of electron-phonon interactions by intense mid-IR pulses [3–5] and photoinduced superconductivity [6,7], THz driving of magnon resonances [8–10], characterization of the interatomic potential of solids [11,12], control of magnetic [13,14], electronic [15,16], and structural [17–23] properties via coherent pumping of phonon resonances.

In the present work we study the ultrafast response of crystalline Bi_2Se_3 to intense THz pulses. This solid belongs to a class of bismuth and antimony chalcogenides, which are objects of intense scientific research in two large areas. First, these crystals demonstrate unique electronic properties predicted for 3D topological insulators [24]. They are narrow-band-gap insulators in the bulk, while the surface hosts Dirac-like electronic states with linear dispersion. These electrons are topologically protected from backscattering and demonstrate spin-momentum locking. Second, a number of crystals from this family ($Bi_2Te_{3-x}Se_x$) demonstrate a large thermoelectric effect [25]. The figure of merit that is used to evaluate their efficiency is inversely proportional to the thermal conductivity [26]. The latter, in turn, is small when the scattering of longitudinal acoustic phonons is strong. In $Bi_2Te_{3-x}Se_x$ materials and several other thermoelectrics (like $Pb_{1-x}Sn_xTe$ [27] and SnSe [26,28]), the efficient scattering channel is provided by TO phonon modes that are considerably softened due to lattice anharmonicity [25]. It is well known that reflectivity spectra of Bi_2Se_3 crystals measured at room temperature contain a relatively intense broad line that appears in the range 60–70 cm^{-1} and is associated with the TO phonon mode of E_u^1 symmetry (reported frequencies are, e.g., 65 cm^{-1} in Ref. [29] or 61 cm^{-1} in Ref. [30]). Therefore, it would be interesting to excite this mode by intense resonant THz radiation and look for nonlinear structural effects.

In the present work we performed such an experiment using nearly single-cycle THz pulses with high peak electric field strength. We found that the optical response of the Bi_2Se_3 crystal to the THz pulse contains oscillations not only at the frequency of E_u^1 mode that was directly excited, but also at the frequencies of three Raman active modes of E_g^1, A_{1g}^1, and E_g^2 symmetry. Recently, observations of THz-induced oscillating signals were reported for Bi_2Se_3, Bi_2Te_3, and Sb_2Te_3 in Refs. [31] and [32]. The appearance of oscillations at the frequency of E_g^2 Raman-active mode was interpreted as vibrationally induced symmetry breaking in the bulk and sum-frequency Raman scattering, respectively. We argue here that the coherent generation of Raman-active modes by an intense THz pulse is a result of lattice anharmonicity and multiphonon processes similar to the sum-frequency ionic Raman scattering proposed in Ref. [23].

II. EXPERIMENTAL DETAILS

The sample used in our experiments was a 24-nm-thick Bi_2Se_3 film grown on a (111)-oriented BaF_2 substrate by molecular beam epitaxy. To reduce the exposure of Bi_2Se_3

*melnikov@isan.troitsk.ru

to ambient air the film was protected by a layer of BaF_2 with a thickness of 28 nm. The details of sample preparation and notes on structural quality of the Bi_2Se_3 film are provided in Supplemental Material [33].

Terahertz pulses with a duration of about 1 ps were generated in a lithium niobate crystal using optical rectification of femtosecond laser pulses with tilted fronts (a description of this method can be found elsewhere [34]). The THz generation stage was fed by 60-fs laser pulses at 800 nm with an average beam power in the range 0.15–1.2 W (i.e., 0.15–1.2 mJ per pulse at 1-kHz repetition rate). Dry nitrogen was continuously pumped through the setup to reduce absorption by water molecules (except measurements with spectrally selective excitation that were done in air). The waveform of the THz pulses was characterized by means of electro-optic detection in a 0.3-mm-thick 110-cut ZnTe crystal. THz radiation was focused into the sample using parabolic mirrors and the resulting peak electric field strength was roughly estimated as $\sim$0.4 MV/cm. To make that estimate we used the well-known formula $E = \sqrt{2I/c\varepsilon_0}$, where E and I are the electric field strength and the intensity of radiation, respectively, that was modified to take into account the real temporal shape of the THz pulse. The corresponding procedure is described in Ref. [35] (a similar approach was reported in Ref. [36]) and corrects the factor of 2 that would be valid for a sine wave. The pulse energy was measured by a pyroelectric detector and was $\sim$1 μJ for a 1.2-mJ fs laser pulse. This gives laser-to-THz conversion efficiency of $\sim 10^{-3}$, which is typical for the tilted pulse front technique in this range of energies and pulse durations. The $1/e^2$ radius of the focused THz beam was estimated as 0.6 mm with the knife-edge technique.

In the experiments we detected transient anisotropic and isotropic changes of transmittance of the sample caused by pump THz pulses. For that purpose we used weak 60-fs probe pulses with a central wavelength of 800 nm. For anisotropic detection the polarization of probe pulses before the sample was set to 45° relative to the vertical polarization of pump THz pulses. Both pump and probe beams were almost normal to the sample surface. Passing through the sample excited by THz radiation the probe pulses experienced a small rotation of polarization, which was detected by measuring the intensities of two orthogonal polarization components of the probe beam I_x and I_y using a Wollaston prism and a pair of photodiodes placed after the sample. The dependence of the value $1-I_x/I_y$ on the probe delay time represented the anisotropic photoinduced response of Bi_2Se_3. To detect isotropic changes of transmittance we used the standard pump-probe layout, in which the first photodiode measured the intensity of probe pulses, while the second photodiode registered reference pulses that did not pass through the sample. As a result, the relative change of transmittance $\Delta T/T$ as a function of the probe delay time was obtained.

III. RESULTS AND DISCUSSION

As follows from the reflectance spectrum of our Bi_2Se_3/BaF_2 sample (Fig. S4 of Supplemental Material [33]), the absorption line that corresponds to the E_u^1 phonon mode is located near 67 cm^{-1} (2 THz). The amplitude of this line is independent of the polarization of light due to the D_{3d}^5 symmetry of bulk Bi_2Se_3. A typical waveform and the corresponding spectrum of the pump THz pulse are shown in Fig. 1. One can see that near 2 THz the spectral amplitude of radiation is large and therefore the E_u^1 mode can be coherently driven by the electric field irrespective of sample orientation (the atomic motion will follow the direction of the electric field vector).

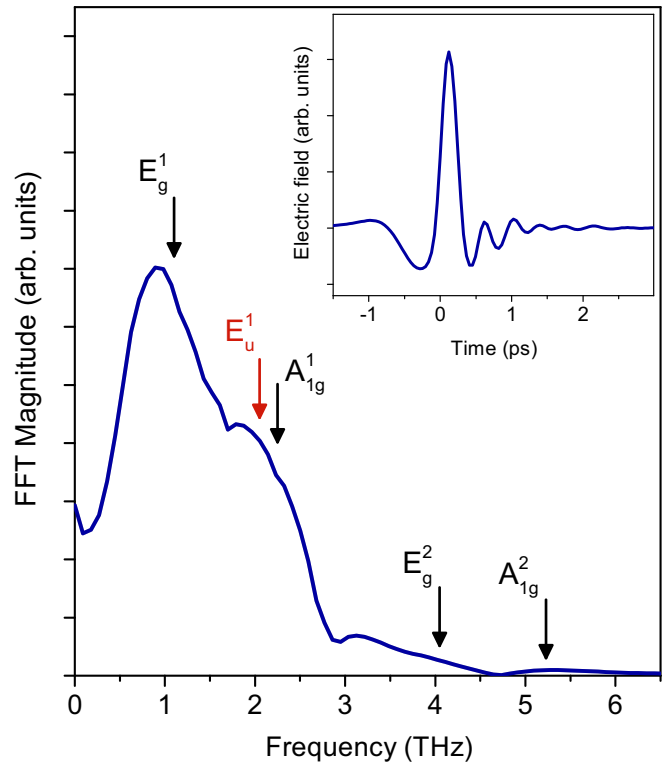

FIG. 1. Time profile of the pump THz pulse (in the inset) and its spectrum obtained using FFT. Arrows show the position of relevant phonon modes of Bi_2Se_3 on the frequency scale.

The transient changes of transmittance of the sample (isotropic detection) and transient polarization rotation (anisotropic detection) are illustrated by Fig. 2. In each case the THz-induced response consists of a monotonic and an oscillating component. The former can be ascribed to the relaxation of electrons excited by the pump THz pulse, while the latter is due to coherent motion of atoms of Bi_2Se_3 that are commonly referred to as coherent phonons [37–46]. We treat the contribution of BaF_2 to the measured traces as negligible, since reference experiments with clean BaF_2 substrates revealed no signal above the noise level.

Typically the amplitudes of oscillations in the photoinduced response that are associated with coherent phonons are treated as being proportional to the corresponding coherent amplitudes of atomic oscillations [37]. In order to find frequencies contained in the oscillating component we applied fast Fourier transform to the time-domain data. To reduce noise and artifacts in the frequency domain we measured decay traces several times using different sampling intervals (i.e., steps of the delay line). Fast Fourier transform (FFT) spectra of individual traces were then averaged to produce spectra shown in Fig. 3. It is possible to distinguish clearly three peaks in the spectrum of the anisotropic signal (1.1, 2.05, and 4.05 THz)

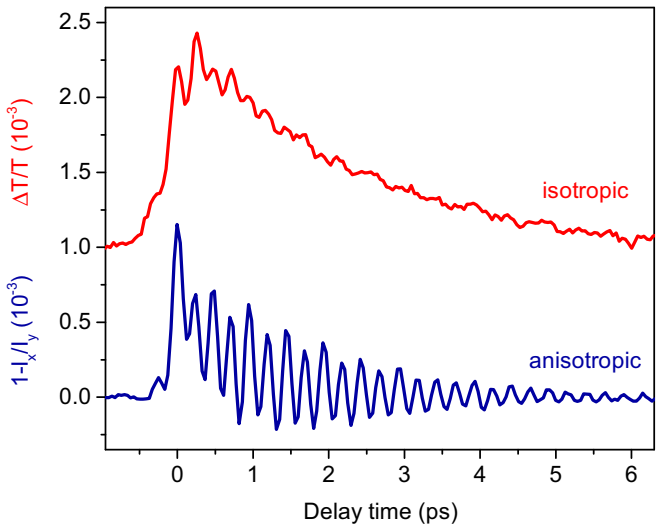

FIG. 2. Response of the Bi_2Se_3 film to the pump THz pulse measured using isotropic ($\Delta T/T$ denotes relative change of transmittance; the curve is shifted upward by 10^{-3}) and anisotropic detection.

and two peaks in the spectrum of the isotropic signal (2.25 and 4.05 THz). We assign these spectral lines to the E_g^1 (1.1 THz), E_u^1 (2.05 THz), A_{1g}^1 (2.25 THz), and E_g^2 (4.05 THz) phonon modes of Bi_2Se_3 [29,47].

It should be noted that, ideally, the anisotropic detection setup is able to register only coherently excited non-fully symmetric modes (E_g and E_u^1 modes in our case), while the isotropic one detects only fully symmetric modes (A_g modes). Fully symmetric coherent phonons induce isotropic variations of reflectivity and/or transmittance and the polarization state of the probe pulse remains unchanged. Therefore, the oscillations are canceled out upon anisotropic detection. Non-fully symmetric oscillations, in contrast, alter the refractive index of the sample in such a way that the polarization of the probe pulse rotates and its intensity is unaffected. The origin of the residual

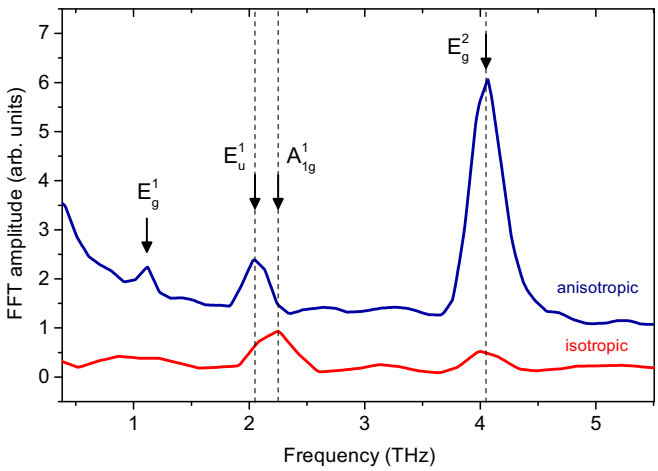

FIG. 3. Spectra of oscillations in the anisotropic and isotropic THz-induced response of Bi_2Se_3. The anisotropic spectrum was shifted upward to facilitate comparison. Arrows illustrate attribution of the observed spectral lines to phonon modes of the crystal.

signal at the E_g^2 frequency in the isotropic response in Fig. 3 can be associated with polarization-sensitive optical elements (in particular, metallic mirrors) that guide probe beam to the photodiode.

We start the analysis of the observed frequency components from the interpretation of the signal at 2.05 THz in the anisotropic response. Since the corresponding E_u^1 mode is IR active, damped oscillations of polarization that follow its coherent excitation by the THz pulse can reveal themselves through the linear electro-optic (Pockels) effect and be detected in our experimental layout. However, Pockels effect in bulk Bi_2Se_3 is forbidden by symmetry due to the presence of the center of inversion. It is nevertheless allowed at the surface of the crystal, which has $C_{3v}(3m)$ symmetry. According to this model, if the sample is nonexcited, the thin layer of Bi_2Se_3 in the vicinity of the Bi_2Se_3/BaF_2 interface can be treated as a uniaxial nonlinear crystal. Excitation of coherent atomic E_u^1 oscillations is equivalent to the application of the external electric field perpendicular to the optical axis of this nonlinear crystal. As a result, the index ellipsoid of the latter is deformed and a certain difference Δn appears between refractive indices experienced by vertically and horizontally polarized components of the probe light. This Δn is then indirectly detected in the anisotropic layout. Thus, the amplitude of the registered oscillations at the E_u^1 frequency $A(E_u^1)$ must demonstrate linear dependence on the electric field strength of the THz pulse E_{THz}, provided the latter is not so strong that effects of saturated absorption are significant. Moreover, the dependence of $A(E_u^1)$ on sample orientation must be in accordance with the C_{3v} symmetry of Bi_2Se_3 surface. We performed model calculations (see the details in Supplemental Material, Sec. 2 [33]) and found that in case of the electro-optic origin of the signal at 2.05 THz its amplitude $A(E_u^1) \propto |\sin 3\varphi|$, where φ is the sample rotation angle.

We measured the dependence of $A(E_u^1)$ on sample orientation (for φ in the range 0–120°) and on the power $P_{800\,\mathrm{nm}}$ of the 800-nm laser beam that was fed into the THz generation stage. The results are shown in Fig. 4 and Fig. 5. It was found that $A(E_g^2)$ is almost independent of φ, while $A(E_u^1)$ is strongly modulated and approximately follows the predicted $A(E_u^1) \propto |\sin 3\varphi|$ dependence. The invariance of E_g^2 amplitude is the consequence of D_{3d}^5 symmetry of the bulk Bi_2Se_3 as soon as for such crystals the intensities of Raman lines do not depend on the orientation of crystallographic axes in the geometry used in our measurements [48]. As follows from Fig. 5(a), the dependence of $A(E_u^1)$ on laser power can be relatively well fitted by a square-root function: $A(E_u^1) \propto \sqrt{P_{800\,\mathrm{nm}}}$. In the optical rectification technique the intensity of THz pulses I_{THz} is proportional to $P_{800\,\mathrm{nm}}$ in a rather wide range. Since $E_{\mathrm{THz}} \propto \sqrt{I_{\mathrm{THz}}}$, the observed root dependence of $A(E_u^1)$ on $P_{800\,\mathrm{nm}}$ implies its linear variation with E_{THz}. Thus, relying on the obtained data, we can conclude that E_u^1 mode is excited across the whole volume of the Bi_2Se_3 film, and the corresponding signal at 2.05 THz originates from the Bi_2Se_3/BaF_2 interfaces through electro-optic modulation of the refractive index associated with surface electronic states of Bi_2Se_3.

In contrast to the E_u^1 mode, E_g^1, A_{1g}^1, and E_g^2 phonon modes of Bi_2Se_3 are Raman but not IR active, and coherent oscillations of atoms at the corresponding frequencies cannot

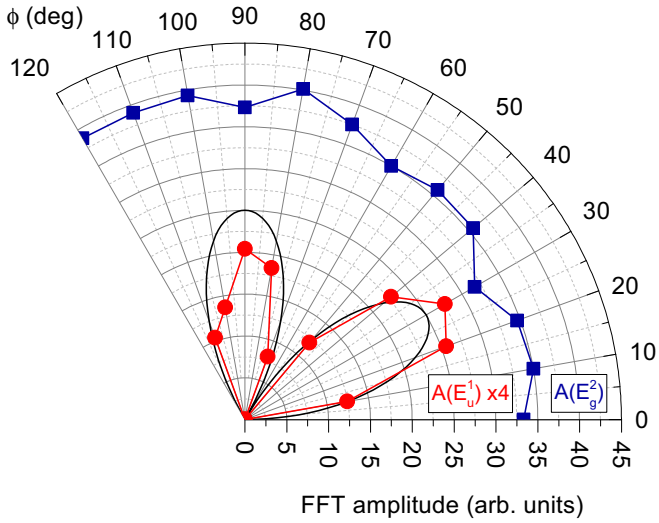

FIG. 4. Dependence of the oscillation amplitudes $A(E_u^1)$ (multiplied by 4, circles) and $A(E_g^2)$ (squares) on the sample orientation. The angle between THz pump and 800-nm probe polarizations was kept constant (45°). The solid line is the $r = a|\sin 3\varphi|$ function with an arbitrarily chosen amplitude a.

be excited directly through resonant linear absorption of the THz radiation (as, for example, in tellurium [49]). Coherent excitation of Raman phonons in solids is commonly described using impulsive stimulated Raman scattering (ISRS) [50], transiently stimulated Raman scattering (TSRS) [51], or displacive excitation of coherent phonons (DECP) [52] theories, but those mechanisms are inefficient in Bi_2Se_3 because the duration of THz pulses in our case is about 1 ps, which is almost equal to (for E_g^1 mode) or considerably larger (for other modes) than the periods of the phonon modes.

In order to interpret the observed phenomenon, the features of coherent oscillations at 2.05 and 4.05 THz (E_u^1 and E_g^2 modes) should be considered, in particular, the relative variation of their amplitudes $A(E_u^1)$ and $A(E_g^2)$ with

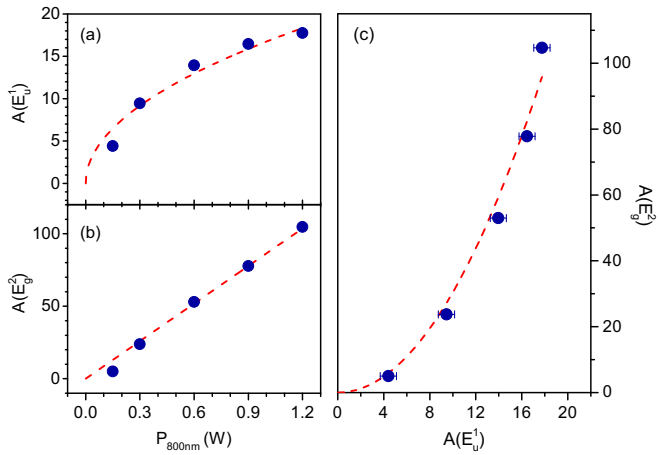

FIG. 5. (a), (b) The dependence of oscillation amplitudes $A(E_u^1)$ and $A(E_g^2)$ on the power of the laser beam fed into the THz generation stage ($P_{800\text{ nm}}$). (c) The dependence of $A(E_g^2)$ on $A(E_u^1)$. Dashed lines represent fits of the experimental data: square root in panel (a), linear in (b), and parabolic in (c).

pump THz electric field. Indeed, we found that while E_u^1 coherent amplitude increases linearly with the THz electric field strength, the E_g^2 one demonstrates quadratic growth [i.e., linear in $P_{800\text{ nm}}$, Fig. 5(b)]. The point measured at $P_{800\text{ nm}} = 0.15$ W deviates from the trend, but the same deviation can be seen in Fig. 5(a) for the first point of the $A(E_u^1)$ power dependence. Nevertheless, if we plot $A(E_g^2)$ as a function of $A(E_u^1)$, the obtained data set can be fitted by a parabola within the experimental error [Fig. 5(c)].

This nonlinear relation between $A(E_u^1)$ and $A(E_g^2)$ implies that some second-order process should be responsible for the generation of coherent E_g^2 phonons. A straightforward way to interpret the observations is to suppose that this process is the three-phonon interaction due to lattice anharmonicity, when two E_u^1 phonons annihilate producing one E_g^2 phonon. This process is allowed by symmetry, because the interaction can be described by the term $\propto q_I^2 q_R$ in the oscillator energy (where q_I and q_R are coordinates of the infrared-active and Raman-active oscillators, respectively), and for the D_{3d} point group $E_u \otimes E_u = A_{1g} + A_{2g} + E_g$. In addition, energy is conserved in this process, as soon as the frequency of E_g^2 mode is approximately twice the frequency of E_u^1 mode. We note here that recently lattice anharmonicity was invoked to explain THz excitation of Raman-active modes in $CdWO_4$ [53].

In case of Bi_2Se_3 the excitation of coherent Raman phonons can be modeled using the approach similar to the one proposed in Ref. [17]. Let $q_I(t)$, $q_R(t)$ and m_I, m_R be coordinates and masses of the infrared-active (I) and Raman-active (R) oscillators, respectively. Then the corresponding equations of motion will have the form

$$m_I \ddot{q}_I = -\frac{\partial}{\partial q_I}(U - Bq_I E_{\text{THz}}(t)), \tag{1}$$

$$m_R \ddot{q}_R = -\frac{\partial}{\partial q_R} U, \tag{2}$$

where

$$U = \tfrac{1}{2} m_I \omega_I^2 q_I^2 + \tfrac{1}{2} m_R \omega_R^2 q_R^2 - A q_I^2 q_R \tag{3}$$

is the potential energy of oscillators including the anharmonic interaction energy $-Aq_I^2 q_R$. For the sake of simplicity we neglect the damping. The term $-Bq_I E_{\text{THz}}(t)$ accounts for the interaction of the IR-active oscillator with the electric field of the pump THz pulse, and B is a constant that characterizes the strength of this interaction. After differentiation we obtain

$$m_I \ddot{q}_I + m_I \omega_I^2 q_I = 2A q_I q_R + B E_{\text{THz}}(t), \tag{4}$$

$$m_R \ddot{q}_R + m_R \omega_R^2 q_R = A q_I^2. \tag{5}$$

We consider the amplitude of THz-driven IR-active oscillator to be much larger than that of the Raman-active oscillator ($q_I \gg q_R$) and neglect the term $2Aq_I q_R$. Then, making the substitution $q_I = \sqrt{m_I m_R}\, Q_I$, $q_R = m_I Q_R$, and $B/m_I^{3/2} m_R^{1/2} \to B$ we get

$$\ddot{Q}_I + \omega_I^2 Q_I = B E_{\text{THz}}(t), \tag{6}$$

$$\ddot{Q}_R + \omega_R^2 Q_R = A Q_I^2. \tag{7}$$

Since damping is neglected, we put to a certain approximation that after the resonant action of the THz pulse $Q_I(t) \propto \cos(\omega_I t)$. Then the driving term AQ_I^2 contains two contributions: the first one is constant, while the second one is $\propto \cos(2\omega_I t)$. The quasiconstant driving force (in fact, it represents the convolution of a step function and the envelope of the THz pulse) is considered in Ref. [17] as a source of transient lattice displacement by analogy with nonlinear optical rectification. This force, however, can excite Q_R only if $\omega_I \gg \omega_R$, which is not the case for Bi_2Se_3, as its optical phonon modes lie in the THz range and have frequencies of the same order. Nevertheless, coherent Raman phonons can be resonantly excited by the second term $\propto \cos(2\omega_I t)$ if $\omega_R = 2\omega_I$, and in Bi_2Se_3 this condition is fulfilled, as soon as $\omega(E_g^2) \approx 2\omega(E_u^1)$.

In order to better illustrate this model we solved numerically the equations of motion for the IR-active and Raman-active oscillators using the real temporal profile of pump THz pulses as the driving force. For that purpose we introduced damping into Eqs. (6) and (7) so that

$$\ddot{Q}_I + \gamma_I \dot{Q}_I + \omega_I^2 Q_I = B E_{\mathrm{THz}}(t), \tag{8}$$

$$\ddot{Q}_R + \gamma_R \dot{Q}_R + \omega_R^2 Q_R = A Q_I^2, \tag{9}$$

where $\omega_I = 2$ THz, $\omega_R = 4$ THz, constants A and B were chosen arbitrarily, while the ratios $\omega_I/\gamma_I \approx 1.5$, $\omega_R/\gamma_R \approx 0.9$—so that the damping of oscillations in the calculated traces was close to the damping observed in the experiment. The results are presented in Fig. 6. Panel (a) contains the THz waveform measured by electro-optic detection. (The same curve is shown in the inset to Fig. 1.) These values were substituted into the right side of Eq. (8) in order to solve it numerically. The obtained solution $Q_I(t)$ is plotted in Fig. 6(b). One can see that after the excitation $Q_I(t)$ represents exponentially decaying oscillations, characteristic of a damped oscillator, and the contribution of transient processes is negligible. We used this $Q_I(t)$ to calculate the trajectory of the Raman-active oscillator $Q_R(t)$ from Eq. (9). As follows from Fig. 6(c), the Raman-active oscillator demonstrates a delayed ~1-ps response that matches the lifetime of the driving force $Q_I^2(t)$.

In order to compare this model to the experimental results we tried to extract oscillating waveforms that correspond to the coherent atomic motions at 2 and 4 THz from the anisotropic response. For that purpose we convolved the latter with wavelet functions at carrier frequencies of 2 and 4 THz, while the duration of the wavelets was 600 and 400 fs, respectively. Such values were chosen in an attempt to keep both temporal and frequency resolution. These wavelets are shown in Fig. 7 along with the results of the convolution.

Figure 7(b) shows that coherent oscillations at 4 THz are launched with a delay and reach the maximal amplitude approximately 1 ps after excitation, similar to the trajectory of the Raman-active oscillator presented in Fig. 6(c). However, the trace at 2 THz in Fig. 7(a) demonstrates a considerable difference from its counterpart $Q_I(t)$ in Fig. 6(b) in the vicinity of zero delay time. The difference is due to the rather intense waveletlike signal that results from the convolution of the 2-THz wavelet with the zero time spike in the anisotropic response (see Fig. 2). This spike not necessarily corresponds to the motion of atoms of Bi_2Se_3 and can be caused by some short-lived purely electronic response of the sample to the THz pulse (e.g., via Kerr effect). When we plot the squared 2-THz trace along with the 4-THz trace as shown in Fig. 7(b), the resulting picture is rather similar to the one obtained above by solving equations of motion for corresponding oscillators [Fig. 6(c)], if one neglects this intense signal near zero delay time. Thus, the results of numerical modeling and time-frequency analysis of the experimental data speak in favor of our assumption that highly excited anharmonic E_u^1 lattice vibrations provide the force that generates coherent Raman-active phonons through anharmonic coupling.

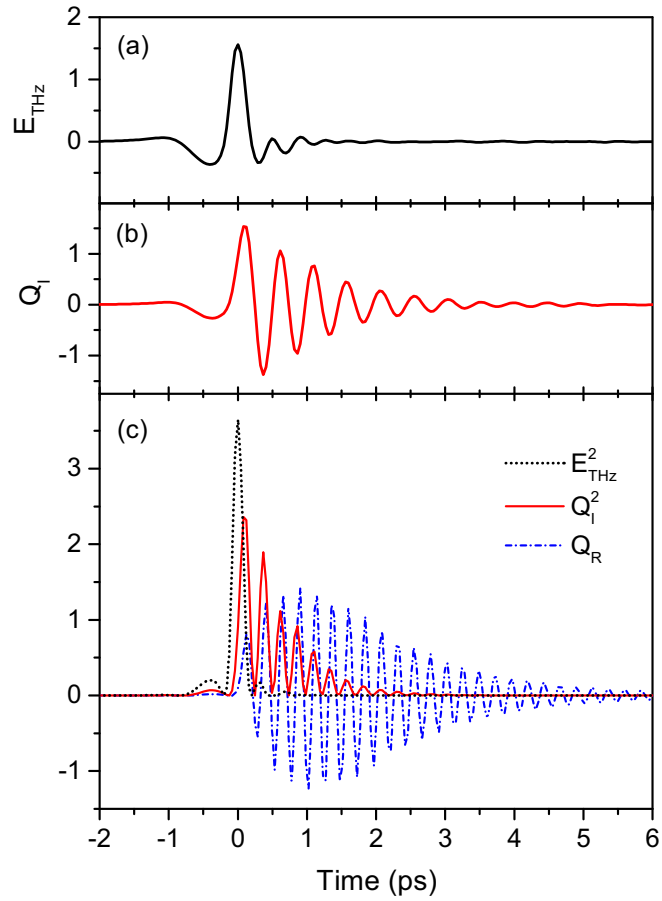

FIG. 6. (a) Electric field of the pump THz pulse substituted as a driving force into Eq. (8). (b) Trajectory of the IR-active oscillator obtained solving Eq. (8). (c) Trajectory of the Raman-active oscillator driven by Q_I^2, the solution of Eq. (9) (dash-dotted curve). The dotted curve represents the squared electric field of the THz pulse as a reference.

Relying on the obtained time-domain data we can rule out the sum-frequency "photonic" Raman scattering as the possible mechanism of coherent generation of E_g^2 phonons. Indeed, in that case the force is $\sim E_{\mathrm{THz}}^2(t)$ and the corresponding waveform is represented mainly by the large central peak that has full width at half maximum of ~200 fs [the dotted curve in Fig. 6(c)]. Therefore, the duration of the force driving the E_g^2 oscillator in the process of sum-frequency "photonic" excitation would be ~200 fs. This is incompatible with the observed ~1-ps growth of the coherent E_g^2 amplitude observed in our work.

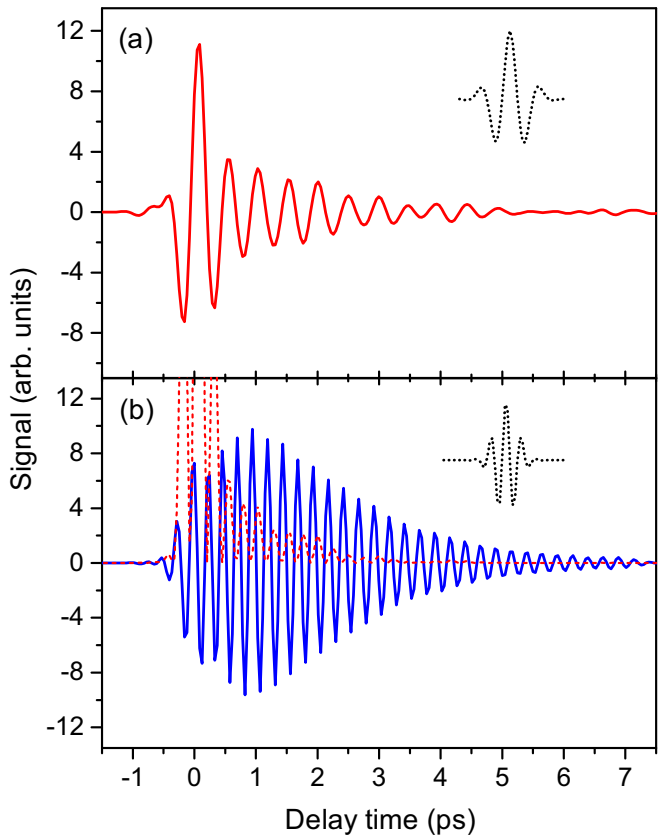

FIG. 7. (a) Convolution of the experimental anisotropic response of Bi_2Se_3 with the wavelet at 2 THz having a duration of ~600 fs. (b) Convolution of the same anisotropic signal with the wavelet at 4 THz having a duration of ~400 fs. The dashed line is the squared trace from panel (a). The wavelets are shown as dotted curves.

We note that a similar conclusion was made recently in the theoretical study [23] of a different material. In that work the authors modeled the action of forces $\sim E^2_{\mathrm{THz}}(t)$ and $\sim Q^2_I(t)$ in the crystal of $BiFeO_3$ excited by THz pulses. As in the case of Bi_2Se_3 the same 1:2 relation exists between the frequencies of the directly driven mode and the Raman-active mode, which is a necessary condition both for the sum-frequency photonic Raman scattering and the excitation due to anharmonic coupling (the latter process is referred to as sum-frequency ionic Raman scattering in Ref. [23]). It was found that the contribution of the force $\sim E^2_{\mathrm{THz}}(t)$ to the resulting coherent amplitude of the Raman active mode is negligible and the principal process is the sum-frequency ionic Raman scattering.

The gradual picosecond growth of the amplitude of E^2_g coherent phonons observed in our work contradicts the model of sum-frequency (photonic) Raman scattering proposed in Ref. [32] for Bi_2Te_3 and Sb_2Te_3. According to the latter the nature of generation process is displacive and the oscillations start almost immediately upon the arrival of the pump THz pulse without any delay. Another notable difference between the results of the work in Ref. [32] and our measurements is the absence of oscillations at the frequency of IR-active mode (at half the frequency of the E^2_g mode) in the traces presented in Ref. [32]. A possible explanation of this difference is the different quality of the samples. Indeed, as one can infer from Ref. [32], the epitaxial films of Bi_2Te_3 and Sb_2Te_3 on Si used there were not protected. From our experience it follows that protection of the Bi_2Se_3 layer is crucial for the correct observation of the THz-induced coherent phonons. Indeed, we found that upon exposure of thin Bi_2Se_3 films to air the effect degrades; in particular, the oscillating signal due to the IR-active mode vanishes almost completely.

Interestingly, the author of Ref. [32] observed a very strong reduction of the amplitude of oscillations associated with coherent E^2_g phonons for 34- and 37-nm-thick Bi_2Te_3 and Sb_2Te_3 films as compared to the films of 13- and 15-nm thickness. This fact was used as an evidence that the oscillating signal originates at the film-substrate interface. In our case, however, the E^2_g oscillations are clearly visible for the relatively "thick" Bi_2Se_3 film of 24-nm thickness, while we concluded that the corresponding signal originates from the bulk.

We emphasize here also the difference between our observations and the results reported in Ref. [31]. Similar to our work the authors of Ref. [31] detected oscillations at frequencies near 2 and 4 THz in the photoinduced response of Bi_2Se_3 using, however, a different detection technique—time-resolved second harmonic generation (SHG). Important is the fact that according to our data the damping of the lower-frequency mode is comparable or stronger than the damping of the higher-frequency mode. Moreover, as shown above, the corresponding wave packets are shifted in time domain relative to one another. The opposite is true for the oscillations observed in Ref. [31]. The 2-THz mode has a longer lifetime than the 4-THz one, while oscillations at both frequencies start almost simultaneously upon THz excitation. Thus, it is possible to assume that different phenomena are observed in Ref. [31] and in our work. In our case the oscillations at 4 THz are caused by coherent E^2_g phonons through anisotropic modulation of the refractive index. In Ref. [31] the signal at 4 THz is "derived" from the oscillations of polarization at 2 THz via the second-order nonlinear optical effect, while coherent E^2_g phonons cannot be observed in the SHG response due to symmetry restrictions [45].

We finish the analysis of E^1_u and E^2_g coherent phonons by checking the resonant character of the oscillatory THz response. For that purpose we performed an additional experiment, in which we filtered the pump THz radiation to selectively attenuate the spectral band near 2 THz. We used a crystal of $PrFe_3(BO_3)_4$ that was at hand; however, it is possible to use any other suitable filter. The reflectance spectrum of $PrFe_3(BO_3)_4$ is shown in Fig. 8(c) [54]. At ~1.7 THz the reflectance experiences a sharp drop and remains low near 2 THz.

If we substitute one of the gold mirrors in the pump channel by this crystal, the amplitude of the THz pulse will be reduced by a factor of 1.24, while the spectral amplitude near 2 THz by a factor of ~2. At the same time, as follows from Fig. 9, the amplitude of E^2_g coherent phonons will decrease by a factor of ~4 and not 1.5 as it would be if the response near 4 THz was proportional to the squared electric field strength. This result shows that the second-order lattice response of Bi_2Se_3 is defined by the spectral amplitude of pump THz radiation near 2 THz, or, in other words, requires a resonance with the E^1_u phonon mode.

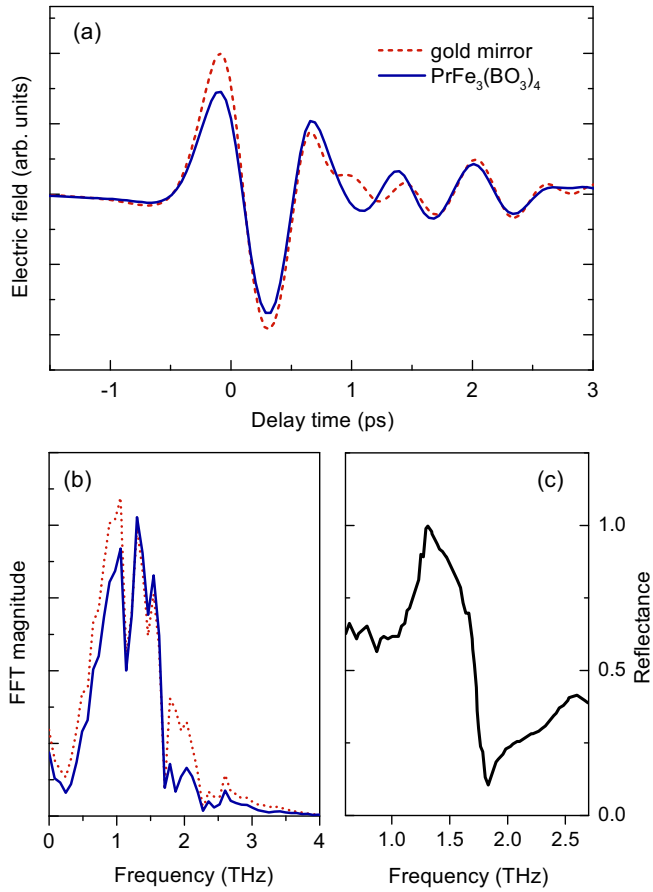

FIG. 8. (a) Electric field of the pump THz pulse reflected from a gold mirror (dashed line) and from the $PrFe_3(BO_3)_4$ crystal (solid). (b) Spectra of the THz waveforms shown in (a). (c) Reflectance spectrum of $PrFe_3(BO_3)_4$ [54]. Measurements were made under ambient conditions.

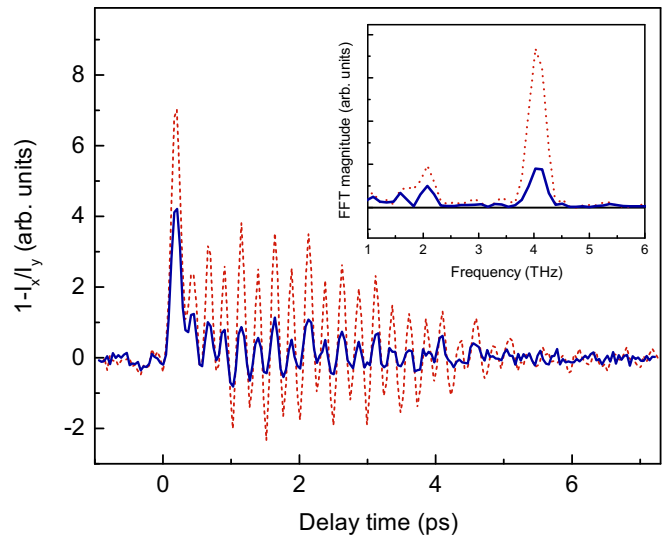

FIG. 9. THz response of Bi_2Se_3 measured using THz pulses reflected from a gold mirror (dashed line) and from the $PrFe_3(BO_3)_4$ crystal (solid line). The inset shows spectra of these signals. Measurements were made under ambient conditions.

Finally, we discuss the origin of E_g^1 and A_{1g}^1 coherent phonons. Excitation of these modes cannot be interpreted taking into account only three-phonon processes by analogy with the generation of E_g^2 mode, because energy is not conserved in this case. However, it is reasonable to consider also four-phonon processes (recently it was proposed that quartic anharmonicity causes anomalous hardening of A_g^1 mode in Bi_2Te_3 [25]). Taking into account the broadening of phonon lines that relaxes to a certain extent the law of energy conservation, it is possible to construct two frequency combinations: $2\omega(E_u^1) \approx \omega(A_{1g}^2) - \omega(E_g^1)$ and $2\omega(E_u^1) \approx 2\omega(A_{1g}^1)$.

The first process implies interaction of two E_u^1, one E_g^1, and one A_{1g}^2 phonons, and, as a result of intense excitation of the E_u^1 mode, generation of coherent oscillations both at 1.1 THz (E_g^1) and 5.23 THz (A_{1g}^2) frequencies. So far we were unable to reliably detect the A_{1g}^2 oscillations in the THz-induced response of Bi_2Se_3, probably because of the relatively long probe pulse. Indeed, its duration was 60 fs—about one-third of the A_{1g}^2 phonon period, which would lead to additional reduction of the oscillating signal amplitude by a factor of ~3 relative to the detection with the ultimate resolution. Another possible reason is that the modulation of the refractive index by A_{1g}^2 phonons is weak, as one can conjecture reviewing the results of pump-probe measurements in the visible and near-infrared domains, where this mode had the smallest amplitude of all detected modes (see, e.g., Ref. [40]).

Nevertheless, the E_g^1 peak is clearly visible in the anisotropic spectra, and we adhere to the model with four-phonon interaction. In this case the anharmonic coupling term in the potential energy will have the form $Aq_I^2 q_{R_1} q_{R_2}$, where indices *1* and *2* refer to the E_g^1 and A_{1g}^2 modes. And, for the equations of motion of the two Raman modes we obtain two coupled equations

$$\ddot{Q}_{R_1} + \omega_{R_1}^2 Q_{R_1} = A Q_I^2 Q_{R_2}, \tag{10}$$

$$\ddot{Q}_{R_2} + \omega_{R_2}^2 Q_{R_2} = A Q_I^2 Q_{R_1}. \tag{11}$$

Analogous to the case of E_g^2 mode discussed above, the driving terms on the right sides of these equations will contain harmonics at combination frequencies of $\omega(A_{1g}^2) - 2\omega(E_u^1)$ and $\omega(E_g^1) + 2\omega(E_u^1)$, and therefore resonantly excite corresponding Raman oscillators.

As for the A_{1g}^1 mode, its anharmonic coupling to the E_u^1 mode will be represented by the term $Aq_I^2 q_R^2$ (interaction of two E_u^1 and two A_{1g}^1 phonons). In this case the equation of motion has the form

$$\ddot{Q}_R + \omega_R^2 Q_R = A Q_I^2 Q_R \tag{12}$$

or

$$\ddot{Q}_R + \left(\omega_R^2 - A Q_I^2\right) Q_R = 0. \tag{13}$$

Again, $AQ_I^2 \propto 1 + \cos 2\omega_I \approx 1 + \cos 2\omega_R$. The constant term causes renormalization of ω_R, while modulation of ω_R at the frequency of $2\omega_R$ excites the oscillator parametrically.

The above simple classical equations for coupled phonon oscillators are used here as a toy model to show the possibility of coherent excitation of the E_g^1, A_{1g}^1, and A_{1g}^2 modes via

quartic anharmonic coupling with the driven E_u^1 mode. When looking at Eqs. (10)–(13) one should bear in mind the quantum nature of lattice vibrations. The latter allows one to model the initial unperturbed motion of each Raman-active oscillator as vibrations with a certain amplitude Q_R that corresponds to the phonon population of the given mode at room temperature. Q_R is nonzero even at zero temperature due to quantum fluctuations. This Q_R is much smaller than the amplitude of the THz-driven IR-active mode Q_I. However, due to the factor Q_I^2 the force $\sim Q_I^2 Q_R$ can be considerable and excite coherent motion with a detectable amplitude. As concerns Eqs. (12) and (13), the term $\sim Q_I^2 Q_R$ acts as an intense modulation of the phonon frequency rather than a force. The nonzero initial Q_R allows parametric excitation of coherent oscillations. We note that the parametric excitation of the Raman-active mode via quartic anharmonic coupling with the driven IR-active mode [as the one described by Eqs. (12) and (13)] was recently considered as a possible process for La_2CuO_4 in Ref. [21].

IV. CONCLUSION

In summary, we have measured the response of a single-crystal Bi_2Se_3 film to a nearly single-cycle THz pulse. We have found that the intense resonant excitation of the IR-active E_u^1 mode leads to the generation of E_g^1, A_{1g}^1, and E_g^2 coherent Raman-active phonons. We conclude that this effect is caused by three- and four-phonon interactions in the anharmonic crystal lattice of Bi_2Se_3. The origin of the force that drives Raman modes is the nonlinear motion of E_u^1 oscillator. The observed effect is similar to the process of sum-frequency ionic Raman scattering proposed in Ref. [23] and differs from conventional Raman scattering, for which the driving term acts only through electronic degrees of freedom. The force $\sim Q_I^2(t)$ is not impulsive like in ISRS, and not displacive like in DECP, but periodic and has a certain duration defined by the THz pulse duration and the damping rate of the driven E_u^1 mode. The observation of picosecond growth of the coherent E_g^2 phonon amplitude allowed us to exclude the sum-frequency photonic Raman scattering as the possible mechanism, because in that case the excitation of the E_g^2 mode would be nearly impulsive.

Coherent E_g^2 phonons should also be generated via this process in related crystals of Bi_2Te_3 and Sb_2Te_3, for which $\omega(E_g^2) \approx 2\omega(E_u^1)$ as in Bi_2Se_3. It would be interesting also to detect other THz-induced coherent Raman-active phonons in the whole family of compounds. Using such control parameters as doping and temperature, it could be possible to investigate the interplay of cubic and quartic lattice anharmonicities in these solids. The approach used here can also be applied for studies of lattice anharmonicities in a broader class of thermoelectrics, many of which have soft TO modes.

ACKNOWLEDGMENTS

The authors thank A. A. Sokolik for useful discussions. This work was supported by the Ministry of Education and Science of the Russian Federation (Project No. RFMEFI61316X0054). The experiments were performed using the Unique Scientific Facility "Multipurpose femtosecond spectroscopic complex" of the Institute for Spectroscopy of the Russian Academy of Sciences.

[1] T. Kampfrath, K. Tanaka, and K. A. Nelson, Resonant and nonresonant control over matter and light by intense terahertz transients, Nat. Photonics **7**, 680 (2013).

[2] D. Nicoletti and A. Cavalleri, Nonlinear light-matter interaction at terahertz frequencies, Adv. Opt. Photonics **8**, 401 (2016).

[3] I. Gierz, M. Mitrano, H. Bromberger, C. Cacho, R. Chapman, E. Springate, S. Link, U. Starke, B. Sachs, M. Eckstein, T. O. Wehling, M. I. Katsnelson, A. Lichtenstein, and A. Cavalleri, Phonon-Pump Extreme-Ultraviolet-Photoemission Probe in Graphene: Anomalous Heating of Dirac Carriers by Lattice Deformation, Phys. Rev. Lett. **114**, 125503 (2015).

[4] E. Pomarico, M. Mitrano, H. Bromberger, M. A. Sentef, A. Al-Temimy, C. Coletti, A. Stöhr, S. Link, U. Starke, C. Cacho, R. Chapman, E. Springate, A. Cavalleri, and I. Gierz, Enhanced electron-phonon coupling in graphene with periodically distorted lattice, Phys. Rev. B **95**, 024304 (2017).

[5] M. A. Sentef, Light-enhanced electron-phonon coupling from nonlinear electron-phonon coupling, Phys. Rev. B **95**, 205111 (2017).

[6] M. Mitrano, A. Cantaluppi, D. Nicoletti, S. Kaiser, A. Perucchi, S. Lupi, P. Di Pietro, D. Pontiroli, M. Riccò, S. R. Clark, D. Jaksch, and A. Cavalleri, Possible light-induced superconductivity in K_3C_{60} at high temperature, Nature (London) **530**, 461 (2016).

[7] D. M. Kennes, E. Y. Wilner, D. R. Reichman, and A. J. Millis, Transient superconductivity from electronic squeezing of optically pumped phonons, Nat. Phys. **13**, 479 (2017).

[8] T. Kubacka, J. A. Johnson, M. C. Hoffmann, C. Vicario, S. de Jong, P. Beaud, S. Grübel, S.-W. Huang, L. Huber, L. Patthey, Y.-D. Chuang, J. J. Turner, G. L. Dakovski, W.-S. Lee, M. P. Minitti, W. Schlotter, R. G. Moore, C. P. Hauri, S. M. Koohpayeh, V. Scagnoli, G. Ingold, S. L. Johnson, and U. Staub, Large-amplitude spin dynamics driven by a THz pulse in resonance with an electromagnon, Science **343**, 1333 (2014).

[9] P. Bowlan, S. A. Trugman, J. Bowlan, J.-X. Zhu, N. J. Hur, A. J. Taylor, D. A. Yarotski, and R. P. Prasankumar, Probing ultrafast spin dynamics through a magnon resonance in the antiferromagnetic multiferroic $HoMnO_3$, Phys. Rev. B **94**, 100404(R) (2016).

[10] S. Baierl, J. H. Mentink, M. Hohenleutner, L. Braun, T.-M. Do, C. Lange, A. Sell, M. Fiebig, G. Woltersdorf, T. Kampfrath, and R. Huber, Terahertz-Driven Nonlinear Spin Response of Antiferromagnetic Nickel Oxide, Phys. Rev. Lett. **117**, 197201 (2016).

[11] A. von Hoegen, R. Mankowsky, M. Fechner, M. Först, and A. Cavalleri, Probing the interatomic potential of solids with strong-field nonlinear phononics, Nature (London) **555**, 79 (2018).

[12] B. S. Dastrup, J. R. Hall, and J. A. Johnson, Experimental determination of the interatomic potential in $LiNbO_3$ via ultrafast lattice control, Appl. Phys. Lett. **110**, 162901 (2017).

[13] T. F. Nova, A. Cartella, A. Cantaluppi, M. Foerst, D. Bossini, R. V. Mikhaylovskiy, A. V. Kimel, R. Merlin, and A. Cavalleri, An effective magnetic field from optically driven phonons, Nat. Phys. **13**, 132 (2017).

[14] D. M. Juraschek, M. Fechner, A. V. Balatsky, and N. A. Spaldin, Dynamical multiferroicity, Phys. Rev. Mater. **1**, 014401 (2017).

[15] M. Rini, Ra. Tobey, N. Dean, J. Itatani, Y. Tomioka, Y. Tokura, R. W. Schoenlein, and A. Cavalleri, Control of the electronic phase of a manganite by mode-selective vibrational excitation, Nature (London) **449**, 72 (2007).

[16] V. Esposito, M. Fechner, R. Mankowsky, H. Lemke, M. Chollet, J. M. Glownia, M. Nakamura, M. Kawasaki, Y. Tokura, U. Staub, P. Beaud, and M. Först, Nonlinear Electron-Phonon Coupling in Doped Manganites, Phys. Rev. Lett. **118**, 247601 (2017).

[17] M. Först, C. Manzoni, S. Kaiser, Y. Tomioka, Y. Tokura, R. Merlin, and A. Cavalleri, Nonlinear phononics as an ultrafast route to lattice control, Nat. Phys. **7**, 854 (2011).

[18] A. Subedi, Proposal for ultrafast switching of ferroelectrics using midinfrared pulses, Phys. Rev. B **92**, 214303 (2015).

[19] D. M. Juraschek, M. Fechner, and N. A. Spaldin, Ultrafast Structure Switching Through Nonlinear Phononics, Phys. Rev. Lett. **118**, 054101 (2017).

[20] R. Mankowsky, M. Först, T. Loew, J. Porras, B. Keimer, and A. Cavalleri, Coherent modulation of the $YBa_2Cu_3O_{6+x}$ atomic structure by displacive stimulated ionic Raman scattering, Phys. Rev. B **91**, 094308 (2015).

[21] A. Subedi, A. Cavalleri, and A. Georges, Theory of nonlinear phononics for coherent light control of solids, Phys. Rev. B **89**, 220301(R) (2014).

[22] S. Maehrlein, A. Paarmann, M. Wolf, and T. Kampfrath, Terahertz Sum-Frequency Excitation of a Raman-Active Phonon, Phys. Rev. Lett. **119**, 127402 (2017).

[23] D. M. Juraschek, and S. F. Maehrlein, Sum-frequency ionic Raman scattering, Phys. Rev. B **97**, 174302 (2018).

[24] M. Z. Hasan and C. L. Kane, Colloquium: Topological insulators, Rev. Mod. Phys. **82**, 3045 (2010).

[25] Y. Tian, S. Jia, R. J. Cava, R. Zhong, J. Schneeloch, G. Gu, and K. S. Burch, Understanding the evolution of anomalous anharmonicity in $Bi_2Te_{3-x}Se_x$, Phys. Rev. B **95**, 094104 (2017).

[26] L.-D. Zhao, S.-H. Lo, Y. Zhang, H. Sun, G. Tan, C. Uher, C. Wolverton, V. P. Dravid, and M. G. Kanatzidis, Ultralow thermal conductivity and high thermoelectric figure of merit in SnSe crystals, Nature (London) **508**, 373 (2014).

[27] O. Delaire, J. Ma, K. Marty, A. F. May, M. A. McGuire, M.-H. Du, D. J. Singh, A. Podlesnyak, G. Ehlers, M. Lumsden, and B. C. Sales, Giant anharmonic phonon scattering in PbTe, Nat. Mater. **10**, 614 (2011).

[28] C. W. Li, J. Hong, A. F. May, D. Bansal, S. Chi, T. Hong, G. Ehlers, and O. Delaire, Orbitally driven giant phonon anharmonicity in SnSe, Nat. Phys. **11**, 1063 (2015).

[29] W. Richter, H. Köhler, and C. R. Becker, A Raman and far-infrared investigation of phonons in the rhombohedral $V_2 - VI_3$ compounds Bi_2Te_3, Bi_2Se_3, Sb_2Te_3 and $Bi_2(Te_{1-x}Se_x)_3 (0 < x < 1)$, $(Bi_{1-y}Sb_y)_2Te_3 (0 < y < 1)$, Phys. Status Solidi B **84**, 619 (1977).

[30] A. D. LaForge, A. Frenzel, B. C. Pursley, T. Lin, X. Liu, J. Shi, and D. N. Basov, Optical characterization of Bi_2Se_3 in a magnetic field: Infrared evidence for magnetoelectric coupling in a topological insulator material, Phys. Rev. B **81**, 125120 (2010).

[31] P. Bowlan, J. Bowlan, S. A. Trugman, R. Valdés Aguilar, J. Qi, X. Liu, J. Furdyna, M. Dobrowolska, A. J. Taylor, D. A. Yarotski, and R. P. Prasankumar, Probing and controlling terahertz-driven structural dynamics with surface sensitivity, Optica **4**, 383 (2017).

[32] L. Braun, *Electron and Phonon Dynamics in Topological Insulators at THz Frequencies* (Freie Universität, Berlin, Germany, 2016).

[33] See Supplemental Material at http://link.aps.org/supplemental/10.1103/PhysRevB.97.214304 for information on sample growth, sample quality and reflectance spectrum, and modeling of the orientation dependence of the E_u^1 signal.

[34] A. G. Stepanov, J. Hebling, and J. Kuhl, Efficient generation of subpicosecond terahertz radiation by phase-matched optical rectification using ultrashort laser pulses with tilted pulse fronts, Appl. Phys. Lett. **83**, 3000 (2003).

[35] T. Ozaki, F. Blanchard, G. Sharma, L. Razzari, X. Ropagnol, F. Vidal, R. Morandotti, J.-C. Kieffer, M. Reid, and F. Hegmann, THz imaging and spectroscopy using intense THz sources at the Advanced Laser Light Source, Phys. Procedia **5**, 119 (2010).

[36] M. D. Thomson, M. Kress, T. Löffler, and H. G. Roskos, Broadband THz emission from gas plasmas induced by femtosecond optical pulses: From fundamentals to applications, Laser Photonics Rev. **1**, 349 (2007).

[37] T. Dekorsy, G. C. Cho, and H. Kurz, Coherent phonons in condensed media, in *Light Scattering in Solids VIII*, edited by M. Cardona and G. Güntherodt (Springer, Berlin, 2000), Chap. 4, pp. 169–209.

[38] N. Kamaraju, S. Kumar, and A. K. Sood, Temperature-dependent chirped coherent phonon dynamics in Bi_2Te_3 using high-intensity femtosecond laser pulses, EPL **92**, 47007 (2010).

[39] J. Qi, X. Chen, W. Yu, P. Cadden-Zimansky, D. Smirnov, N. H. Tolk, I. Miotkowski, H. Cao, Y. P. Chen, Y. Wu, S. Qiao, and Z. Jiang, Ultrafast carrier and phonon dynamics in Bi_2Se_3 crystals, Appl. Phys. Lett. **97**, 182102 (2010).

[40] K. Norimatsu, J. Hu, A. Goto, K. Igarashi, T. Sasagawa, and K. G. Nakamura, Coherent optical phonons in a Bi_2Se_3 single crystal measured via transient anisotropic reflectivity, Solid State Commun. **157**, 58 (2013).

[41] K. Norimatsu, M. Hada, S. Yamamoto, T. Sasagawa, M. Kitajima, Y. Kayanuma, and K. G. Nakamura, Dynamics of all the Raman-active coherent phonons in Sb_2Te_3 revealed via transient reflectivity, J. Appl. Phys. **117**, 143102 (2015).

[42] M. Weis, K. Balin, R. Rapacz, A. Nowak, M. Lejman, J. Szade, and P. Ruello, Ultrafast light-induced coherent optical and acoustic phonons in few quintuple layers of the topological insulator Bi_2Te_3, Phys. Rev. B **92**, 014301 (2015).

[43] O. V. Misochko, A. A. Melnikov, S. V. Chekalin, and A. Yu. Bykov, Features of coherent phonons of the strong topological insulator Bi_2Te_3, JETP Lett. **102**, 235 (2015).

[44] O. V. Misochko, J. Flock, and T. Dekorsy, Polarization dependence of coherent phonon generation and detection in the three-dimensional topological insulator Bi_2Te_3, Phys. Rev. B **91**, 174303 (2015).

[45] A. Y. Bykov, T. V. Murzina, N. Olivier, G. A. Wurtz, and A. V. Zayats, Coherent lattice dynamics in topological insulator Bi_2Te_3 probed with time-resolved optical second-harmonic generation, Phys. Rev. B **92**, 064305 (2015).

[46] E. Golias and J. Sanchez-Barriga, Observation of antiphase coherent phonons in the warped Dirac cone of Bi_2Te_3, Phys. Rev. B **94**, 161113(R) (2016).

[47] W. Cheng, and S.-F. Ren, Phonons of single quintuple Bi_2Te_3 and Bi_2Se_3 films and bulk materials, Phys. Rev. B **83**, 094301 (2011).

[48] H.-H. Kung, M. Salehi, I. Boulares, A. F. Kemper, N. Koirala, M. Brahlek, P. Lošťák, C. Uher, R. Merlin, X. Wang, S.-W. Cheong, S. Oh, and G. Blumberg, Surface vibrational modes of the topological insulator Bi_2Se_3 observed by Raman spectroscopy, Phys. Rev. B **95**, 245406 (2017).

[49] T. Huber, M. Ranke, A. Ferrer, L. Huber, and S. L. Johnson, Coherent phonon spectroscopy of non-fully symmetric modes using resonant terahertz excitation, Appl. Phys. Lett. **107**, 091107 (2015).

[50] L. Dhar, J. A. Rogers, and K. A. Nelson, Time-resolved vibrational spectroscopy in the impulsive limit, Chem. Rev. **94**, 157 (1994).

[51] D. M. Riffe and A. J. Sabbah, Coherent excitation of the optic phonon in Si: Transiently stimulated Raman scattering with a finite-lifetime electronic excitation, Phys. Rev. B **76**, 085207 (2007).

[52] H. J. Zeiger, J. Vidal, T. K. Cheng, E. P. Ippen, G. Dresselhaus, and M. S. Dresselhaus, Theory for displacive excitation of coherent phonons, Phys. Rev. B **45**, 768 (1992).

[53] J. A. Johnson, P. D. Salmans, and N. R. Ellsworth, High-field THz lattice control via anharmonic vibrational coupling, in *International Conference on Ultrafast Phenomena, OSA Technical Digest (online)* (Optical Society of America, 2016), paper UW4A.11.

[54] K. N. Boldyrev, T. N. Stanislavchuk, A. A. Sirenko, L. N. Bezmaternykh, and M. N. Popova, Coupling between phonon and crystal-field excitations in multiferroic $PrFe_3(BO_3)_4$, Phys. Rev. B **90**, 121101 (2014).